Evaluation of an Analytical Design Tool for Ballistic Dynamics Simulation

by

Ashish K. Sareen
Michael R. Smith
Bell Helicopter Textron, Inc.
Fort Worth, Texas

ABSTRACT

Usefulness of ballistic dynamics simulations as a design tool in assessing ballistic tolerance and as an aid in pretest guidance is studied. Accurate simulations of hydraulic ram, including failure mode prediction, can be useful in enhancing survivability and in guiding pretest specimen setup to ensure projectile strike and exit at critical locations, thereby minimizing the cost of expensive development tests. To understand the potential of ballistic simulation as a design tool, MSC/DYTRAN™ code has been evaluated at Bell Helicopter Textron, Inc. by conducting simulations using projectiles of different sizes to impact and penetrate a generic fluid-filled tank and a composite wing structure containing fuel cells. Projectile trajectory, fluid pressures in the fuel tank, and wing structural response from the analysis are compared with the measured data. The physics of the phenomenon appears to be accurately simulated, indicating that MSC/DYTRAN™ could be a useful design tool for enhancing ballistic tolerance.

1996 MSC World User's Conference Proceedings
Newport Beach, CA
June 3–7, 1996

EVALUATION OF AN ANALYTICAL DESIGN TOOL FOR BALLISTIC DYNAMICS SIMULATION

Ashish K. Sareen
Engineering Specialist, Structural Dynamics

Michael R. Smith
Senior Engineering Specialist, Structural Dynamics

Bell Helicopter Textron, Inc.
Fort Worth, Texas

ABSTRACT

Usefulness of ballistic dynamics simulations as a design tool in assessing ballistic tolerance and as an aid in pretest guidance is studied. Accurate simulations of hydraulic ram, including failure mode prediction, can be useful in enhancing survivability and in guiding pretest specimen setup to ensure projectile strike and exit at critical locations, thereby minimizing the cost of expensive development tests. To understand the potential of ballistic simulation as a design tool, MSC/DYTRAN™ code has been evaluated at Bell Helicopter Textron, Inc. by conducting simulations using projectiles of different sizes to impact and penetrate a generic fluid-filled tank and a composite wing structure containing fuel cells. Projectile trajectory, fluid pressures in the fuel tank, and wing structural response from the analysis are compared with the measured data. The physics of the phenomenon appears to be accurately simulated, indicating that MSC/DYTRAN™ could be a useful design tool for enhancing ballistic tolerance.

INTRODUCTION

Accurate design analysis offers the potential to provide significant design enhancements while minimizing the cost of expensive development tests. This is particularly true in the field of ballistic survivability. For aircraft to survive in hostile environments, designers must account for various threats. Among the most important factors in aircraft vulnerability is the ballistic threat to the fuel tank. When a high-speed projectile impacts and penetrates an aircraft fuel tank, an intense pressure wave propagates through the virtually incompressible fluid and impinges upon the tank wall. The results can be catastrophic, causing failure of not only the tank but also of the surrounding structure. This phenomenon is known as hydrodynamic ram, or more commonly, hydraulic ram. Accounting for the effect of hydraulic ram on fuel tanks and the surrounding structure is critical to the design of a ballistically tolerant aircraft.

Presented at the American Helicopter Society 52nd Annual Forum, Washington, D.C., June 4–6 1996.

In order to enhance ballistic design methodology, confidence must be established that the analysis maintains fidelity with the physics of the phenomenon. Because of the dynamic nature of hydraulic ram, which involves changes of state in the fluid and the interaction between structure and fluid, MSC/DYTRAN™ (Ref. 1) is one of the few commercially available codes that is well suited to simulate this phenomenon. MSC/DYTRAN™ is a three-dimensional finite-element analysis code that uses explicit time integration to solve highly nonlinear, large deformation, short-lived transient structural and fluid-structure coupling problems.

This paper presents a methodology for using MSC/DYTRAN™ to simulate the full sequence of hydraulic ram and its attendant structural response. In addition, two simulations are conducted and correlated with measured data from the Design and Manufacture of Low Cost Composites – Bonded Wing (DMLCC–BW) Contract (Ref. 2) in order to provide insight into the potential of this analytical code as an engineering design tool to improve ballistic tolerance and alleviate expensive testing.

ELEMENTS OF HYDRAULIC RAM

Accurate simulation of structural damage requires accurate modeling of the energy transfer from the projectile to the fluid and structure. This requires accurate simulation of projectile kinetics and kinematics, which in turn requires accurate simulation of fluid dynamics as well as fluid-structure interactive dynamics.

Phases of Hydraulic Ram

There are three primary sequential phases in hydraulic ram (Refs. 3 and 4): the shock phase, the drag phase, and the cavitation phase.

Shock Phase. The kinetic impulse or shock phase occurs when the projectile initially penetrates the tank wall and impacts the fluid, producing a hemispherical shock wave. This shock wave propagates at sonic velocity through the fluid away from the projectile–fluid impact point, producing

an impulsive load that acts on the entire surrounding tank wall. This impulse is most destructive close to its point of origin – near the entry hole.

Drag Phase. The projectile is slowed by viscous drag forces as it moves through the fluid. The resulting momentum transfer from the projectile to the fluid increases its kinetic energy, producing a pressure wave with lower intensity than in the shock phase, but with longer duration.

Cavitation Phase. As the projectile moves through the fluid, the fluid is displaced both along the axis of travel and radially to this axis. The radial velocity away from the projectile causes a wake to form at the aft end of the projectile. Behind this wake, a cavity forms where the pressure is below the vapor pressure of the fluid. As this cavity collapses, significant pressure pulses are generated that propagate through the fluid, causing the greatest damage to the opposing wall of the fuel tank, near the exit hole.

Projectile Tumbling

Projectile kinematics contributes significantly to the hydraulic ram effect. If the projectile tumbles in the fluid, the energy transferred from the projectile to the fluid during the drag phase is dramatically increased and the structural loading is correspondingly increased. In addition, a tumbled projectile produces greater cavitation, which in turns produces greater pressure pulses. Pressure waves generated by a projectile in a fully-tumbled attitude, that is, a 90-deg yaw attitude (see Fig. 1), will be approximately five times more intense than those generated by the same projectile in its normal 0-deg yaw attitude (Ref. 5). As shown in Fig. 1, the projectile continues to tumble beyond the 90-deg yaw attitude along its trajectory before assuming a stable attitude.

Each of the three phases of hydraulic ram contributes to structural damage and is therefore critical to account for in ballistic analysis. While previous work simulated the drag and cavitation phases of hydraulic ram, published literature (e.g., Ref. 3) indicates that the initial shock phase of hydraulic ram has not been directly simulated with MSC/DYTRAN™ . Inclusion of this phase in the analysis is important, since significant kinetic energy can be transferred during the initial shock phase. The analysis herein directly simulates all three phases of hydraulic ram.

BALLISTIC DYNAMICS MODELING WITH MSC/DYTRAN™

MSC/DYTRAN™ contains two processing techniques, Lagrangian and Eulerian, which can be coupled.

Structural Modeling (Lagrange)

The Lagrangian method is the most common finite-element processing technique for engineering applications. Grid points are located on the body being analyzed. Elements of material with constant (invariant) mass connect the grid points, forming a mesh. As the body deforms, the grid points move with the body and the elements (mesh) distort. The Lagrangian processor uses explicit formulation and allows large deflection with material and geometric nonlinearities.

Fluid Modeling (Euler)

The Eulerian method is most frequently used for analyzing fluids. The grid points remain fixed in space, defining fixed volumes, or elements. As the fluid moves through these Euler elements, or mesh, the mass, momentum, and energy of the fluid is transported from one element to another. The Eulerian processor is essentially an explicit inviscid computational fluid dynamics code.

Structure–Structure Interaction

The interaction between two separate Lagrangian meshes is provided in MSC/DYTRAN™ to model bearing (including impact) and sliding contact between two structures. For ballistic dynamics, adaptive contact is especially useful.

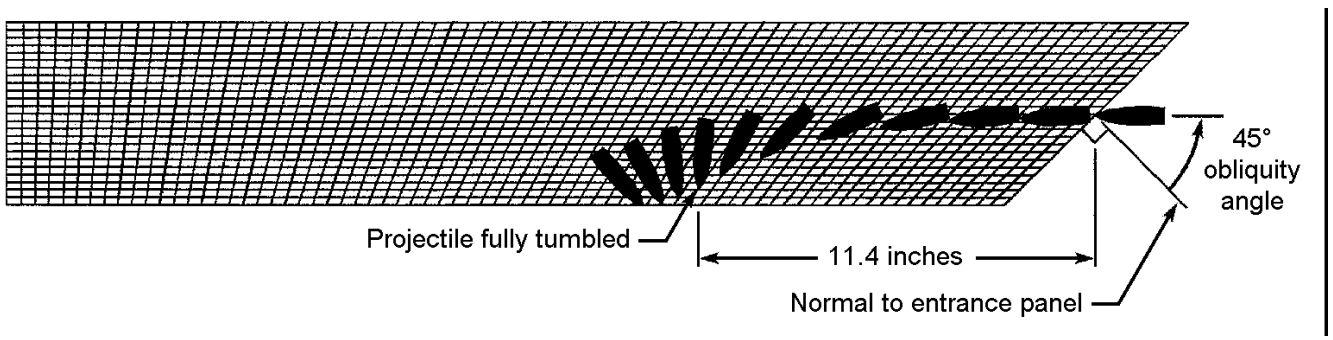

Fig. 1. Tumbling behavior for projectile pentrating at 45-deg obliquity.

Adaptive Contact. Adaptive contact is used to transmit forces between the projectile and the tank. Adaptive contact allows a penetrating object to go through a closed surface after elements in its path have failed, without causing holes in its connectivity. Any contact requires master/slave designations for the contacting surfaces. In the current simulations, the tank wall is designated as the slave surface and the projectile is termed the master surface.

At every time step, MSC/DYTRAN™ checks the adaptive contact for the grid points of the projectile to see if any have penetrated into an element of the tank wall. If penetration is found, a force is applied on the projectile grid in the direction opposite the penetration. An equal and opposite force is also applied to the grids which are connected to the element being penetrated. What makes the contact adaptive is its ability to allow the projectile to punch through the hole created when the elements in front of it have failed. When an element in the contact region fails, the adaptive contact algorithm stops applying force to it (and also stops applying force from it on the penetrating object). This simulates the formation of a hole and allows subsequent penetration to occur unimpeded.

Fluid-Structure Interaction (Coupling)

Lagrangian and Eulerian meshes can be coupled for fluid-structure interaction. MSC/DYTRAN™ provides Arbitrary-Lagrange–Euler (ALE) coupling and general coupling.

ALE Coupling. ALE coupling is used between the tank wall and the fluid. It connects the Eulerian mesh to the Lagrangian mesh, which allows the Eulerian mesh to follow the motion of the Lagrangian mesh as the tank wall deflects. The fluid in the Eulerian elements adjacent to the tank wall is then compressed due to the motion of the wall and exerts a reaction pressure on the tank wall elements. MSC/ DYTRAN™ employs a smoothing algorithm to prevent highly distorted Eulerian elements at the interface between the two meshes.

General Coupling. General coupling is used between the projectile and the fluid to preclude the problem associated with continuous distortion of the Eulerian mesh as the projectile moves through the fluid and exits the tank. General coupling allows arbitrary motion of the Lagrangian structure through the fixed Eulerian mesh. The Lagrangian structure forms a continuously moving flow boundary for the Eulerian fluid while the fluid simultaneously acts as a pressure load on the Lagrangian structure. The general coupling algorithm performs intersection calculations at every time step to determine which Euler volumetric elements are intersected by which Lagrange elements. The code computes the volume fractions of the intersected Euler elements occupied by Lagrangian structure, and applies pressure forces to each intersected Euler element to displace the required amount of fluid out of the element. This pressure is also applied to the intersecting Lagrange element. In contrast with ALE coupling, this approach allows unlimited deformation or movement of the Lagrange structure (necessary in the case of a penetrating projectile); but general coupling also requires a large number of CPU-intensive 3-D intersection calculations at every time step.

An initial penetration of the projectile into the Euler mesh at time step zero is necessary for general coupling to work properly. The general coupling algorithm only checks for penetrated or intersected Euler elements immediately adjacent to those already penetrated. Thus if no elements are initially penetrated, none will be found throughout the entire solution sequence.

BALLISTIC DYNAMICS SIMULATION

In order to access existing ballistic test data, two different tanks are analyzed: a generic tank and a composite wing tank. Projectile tumbling and fluid pressures are correlated with the generic tank, while projectile trajectory and structural response and damage are correlated with the composite wing tank.

Generic Tank

In the early 1970s, ballistic tests were conducted by the Naval Weapons Center (NWC) on a 60-inch (1.52-m) cube test cell (Ref. 6). The water-filled, open-top test cell (Fig. 2) was shot with 12.7 mm API (armor-piercing incendiary) rounds at three different obliquity angles: 0 deg, 30 deg, and 45 deg. Five pressure transducers were positioned in the fluid along the line of shot to measure the pressure time histories. The pressure transducers were placed 6 inches (0.152 m) above the expected trajectory along 6-inch (0.152-m) intervals. Coordinates of the pressure transducers with respect to the test cell are listed in Fig. 2. High-speed motion picture data was taken to determine the projectile tumbling behavior.

The test cell walls were constructed of 1/8-inch-thick (3.2-mm) steel plates with angle iron reinforcements at the edges and an open top. A 1/2-inch (12.7-mm) steel plate at the rear wall prevented projectile exit from the cell. A 2- × 2-ft (0.61- × 0.61-m) entrance panel made of 0.063-inch-thick aluminum was held in place by compression between two rubber gaskets around the edges. Two 1-inch-thick (25.4-mm) plexiglass windows were placed on opposite sides of the cell to allow for high-speed photography.

Fluid Model. The water is modeled with 92,160 Eulerian hydrodynamic elements (solid elements referencing a

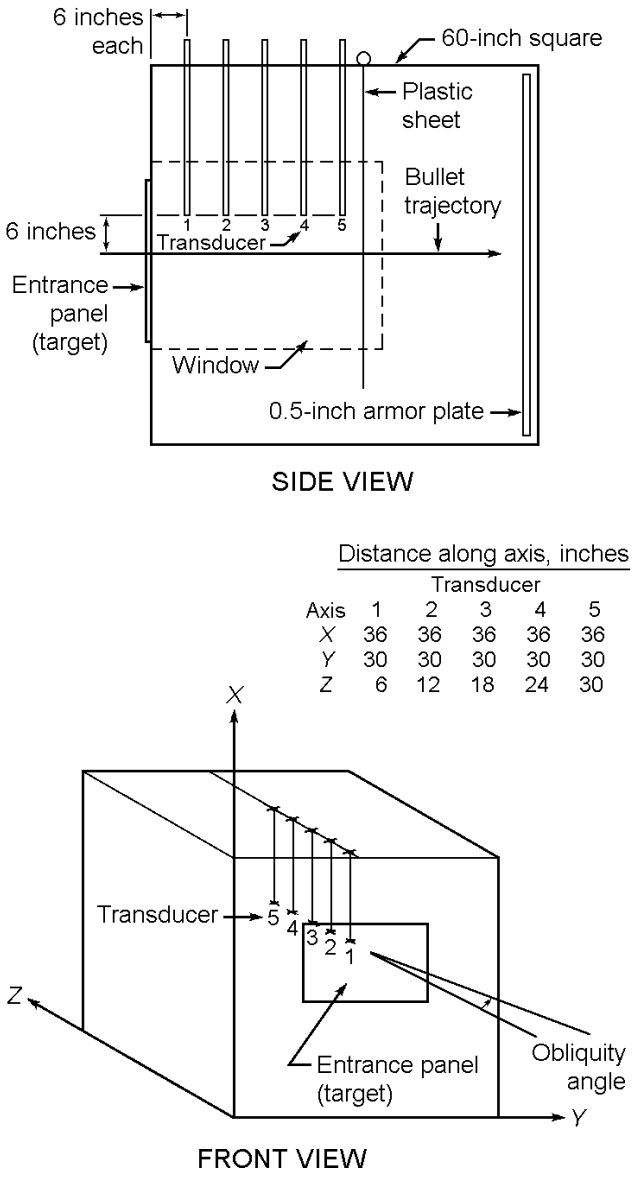

Fig. 2. Test tank – side view and front view (from Ref. 1).

PEULER property). The properties of the water assume no viscosity and are determined from its mass and bulk modulus. The installed memory of the workstation limited the analysis to about 100,000 total elements. To allow finer meshing along the shotline, the back 24 inches (0.61 m) of the tank are not explicitly modeled but are represented by a FLOW boundary. The FLOW boundary allows fluid to move into and out of the Euler mesh across the back surface instead of blocking transport. The FLOW boundary does not reflect pressure waves; rather, it simulates the presence of additional fluid beyond the mesh boundary. Thus, the tank analytical model is 60 inches deep, 60 inches wide, and 36 inches long along the shotline (1.52 m × 1.52 m × 0.76 m).

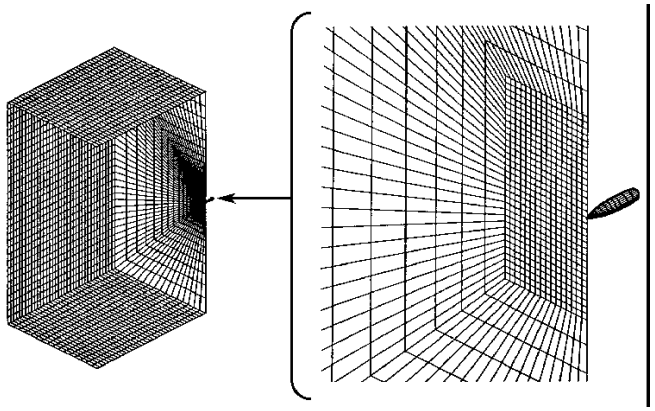

Fig. 3. Comparison of mesh densities of the projectile and the tank.

The Euler mesh shown in Fig. 3 is composed of two distinct regions: a central "core" region, and the surrounding region extending to the tank wall. The core is sized and meshed for each obliquity angle so that the projectile stays within this finely meshed region throughout the analysis. The core region is 8 inches wide by 8 inches deep, and extends 36 inches along the length of the tank (0.20 m × 0.20 m × 0.76 m). The core has a constant mesh density with 36,864 elements (32×32×36). This mesh density yields good results at small projectile angles (i.e., when there is no tumbling) but some problems occur at high yaw angles, because it is possible for the projectile to become completely contained in one row of elements, as shown in Fig. 4. Since MSC/ DYTRAN™ uses first-order approximations, the pressure within each element is assumed to be uniform. Thus when the projectile is fully

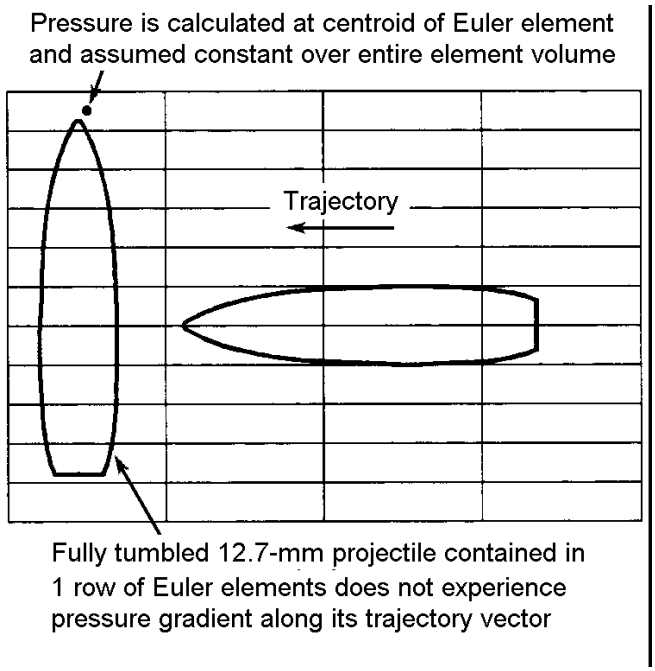

Fig. 4. Example of numerical problem from coarse Euler mesh.

contained in one row of elements, it experiences no pressure gradient along its trajectory vector and therefore no drag force opposing its motion. When the projectile moves into the next row of elements, it experiences a sudden pressure gradient. This causes multiple small pressure waves to be generated, which results in oscillations in the projectile deceleration.

Tank Wall Model. The tank walls (Fig. 3) are modeled with 7,168 Lagrangian shell elements having properties representing the 1/8-inch-thick (3.2-mm) steel plate. The open top is modeled with elements having effectively no stiffness (thickness of 0.0001 inch) and a density equal to water.

Projectile Model. The 12.7-mm projectile (Figs. 3 and 5) is modeled with 312 Lagrangian shell elements. These elements define the shape of the projectile, which is then specified as rigid with a RIGID card in the model. The mass of the projectile was obtained from Ref. 6; however, the moments of inertia had to be computed. Though not available at the time of this analysis, MSC/DYTRAN™ now provides a new feature, MATRIG, which internally calculates mass moments of inertia based on geometry. For non-zero obliquity shots, the deformation of the projectile is simulated in the analysis with 2-deg yaw perturbation and 0-deg yaw velocity for the initial condition at wall penetration.

Analytical Results. The kinetic energy lost by the projectile as it penetrates the generic tank at 0-deg obliquity and travels through the fluid is shown in Fig. 6. During the first phase of hydraulic ram, that is during the initial impact and wall penetration, 3.3% of the total projectile kinetic energy is lost (Fig. 6). Over the next 1.0 milliseconds (ms), the kinetic energy of the projectile is reduced to approximately 45% of its initial impact state. The evident oscillations in the projectile velocity between 0.6 and 0.8 ms (see Fig. 6) are a result of the projectile being contained in one row of elements (see Fig. 4), and indicate that the projectile is in a nearly fully-tumbled state. The calculated distance for the projectile to reach a fully-tumbled state is 18.97 inches (0.4818 m) which is within 14.0% of the measured distance of 17.00 inches (0.4318 m) (Ref. 7).

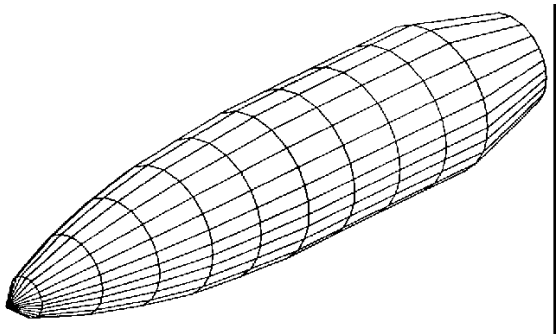

Fig. 5. Hidden-line representation of the projectile model.

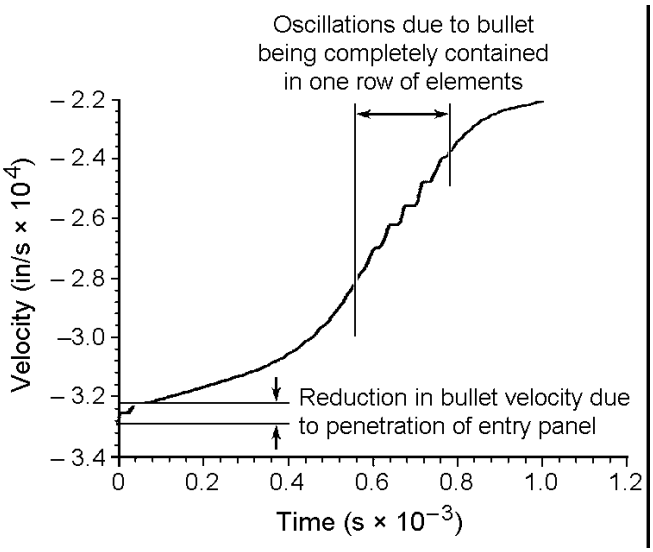

Fig. 6. Projectile velocity time history through generic tank.

The shape of the calculated pressure contours in the fluid is visible in Fig. 7. The calculated peak overpressures in the fluid at the five transducer locations shown in Fig. 2 correlate within approximately 5% of the measured data from the NWC lab tests, as indicated in Table 1 and Fig. 8. The calculated pressure time history corresponding to the fifth transducer (Fig. 9) which is located in the middle of the tank beyond the fully-tumbled projectile position, reveals that, rather than a broad peak, several significant pressure oscillations result from the numerical mesh problem. Mesh refinement in the direction of projectile travel should reduce this behavior and improve the pressure correlation.

As the shotline obliquity increases, projectile tumbling occurs earlier. For projectile penetration at 30 deg, the calculated distance to a fully-tumbled state is 14.2 inches (0.361 m). For 45-deg obliquity, the calculated distance is 11.4 inches (0.290 m) (see Fig. 1). Measured data for non-zero obliquity shots were not available; however, the averaged

Table 1. Correlation of peak pressure for 0-deg shotline obliquity.

	Peak pressure (lb/in^2)				
Pressure transducer:	No. 1	No. 2	No. 3	No. 4	No. 5
MSC/DYTRAN™	375	656	873	846	594
Measured average	357	625	859	801	591
Percentage of difference	5.0%	5.0%	1.6%	5.6%	0.4%

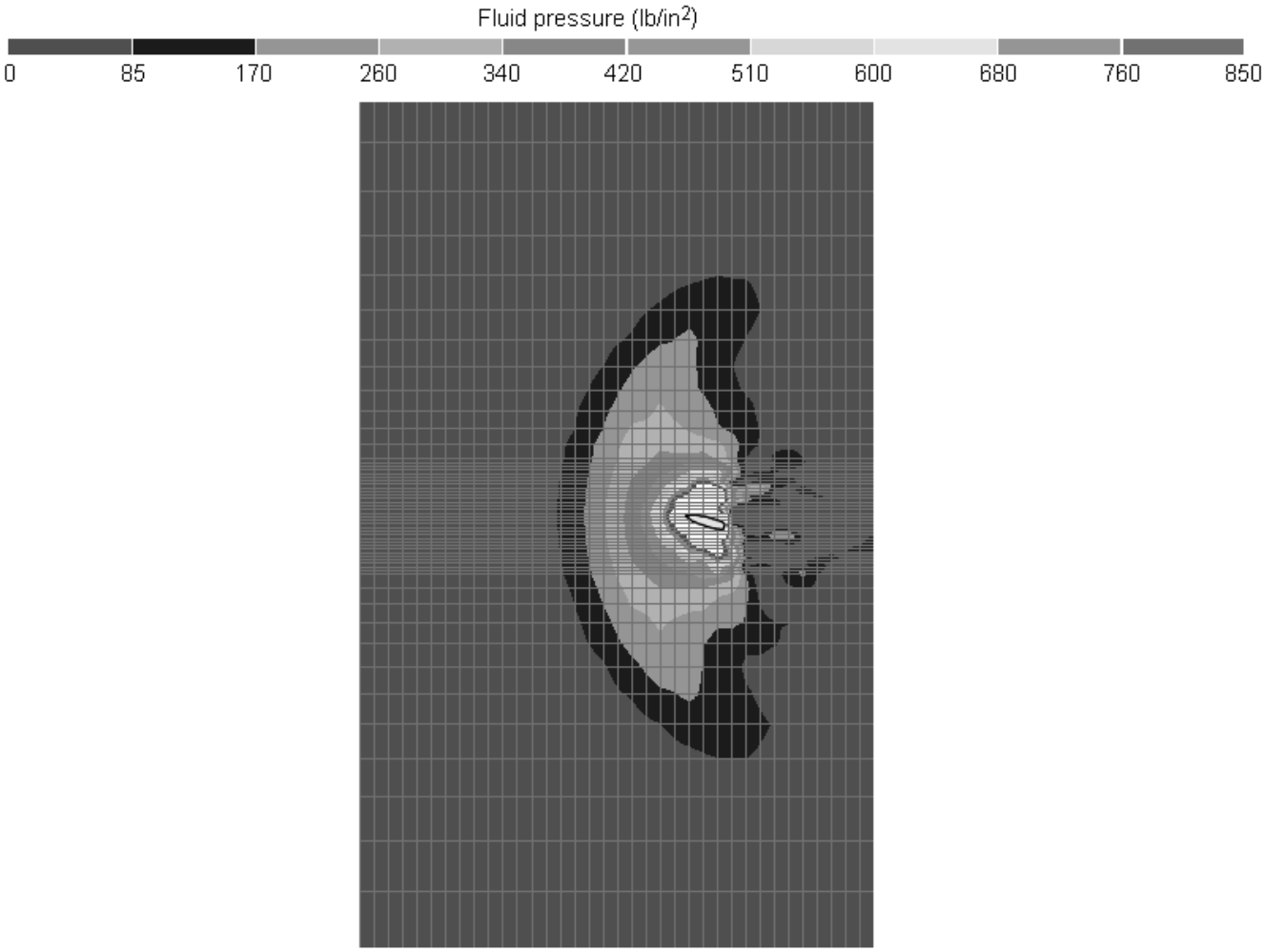

Fig. 7. Pressure contours for a partially tumbled projectile.

analytical predictions contained in Ref. 5 of 13.4 inches (0.340 m) for 30 deg and 11.3 inches (0.287 m) for 45 deg agree exceptionally well with the MSC/DYTRAN™ results.

The peak overpressures calculated by MSC/NASTRAN™ for the 30-deg obliquity case agree reasonably well for the first transducer (Fig. 10). However, as the projectile reaches the subsequent transducers, the error in calculated pressure is significant (see Fig. 11 for fluid pressure at the fifth transducer), indicating the problem with a coarse mesh is aggravated when the projectile tumbles with greater kinetic energy. This effect is even more pronounced at 45-deg obliquity, as shown in Fig. 12.

Correlation of results from the generic tank indicates that MSC/DYTRAN™ can accurately simulate the observed projectile trajectory and shows promise in accurately simulating fluid pressures.

Composite Wing Tank

The composite wing structure (Fig. 13) is composed of bonded rib-to-skin attachment with cocured stringer and spar caps made of bundled pultruded carbon epoxy rods to provide superior stiffness along the length of composite wing skin (Ref. 8). While these mostly-bonded wing structures have the potential of cost and weight savings, their implementation into future military aircraft is contingent on their suitability in providing the necessary structural integrity to survive hydraulic ram. Accordingly, ballistic testing was required to demonstrate that the new composite wing construction was robust to hydraulic ram. Ballistic tests were conducted at Bell Helicopter Textron, Inc. to assess the relative performance of these bonded wings (Ref. 9). These tests used small and large bore armor-piercing (AP) projectiles. Three tests have been completed with more planned. If the simulation results correlate well with the

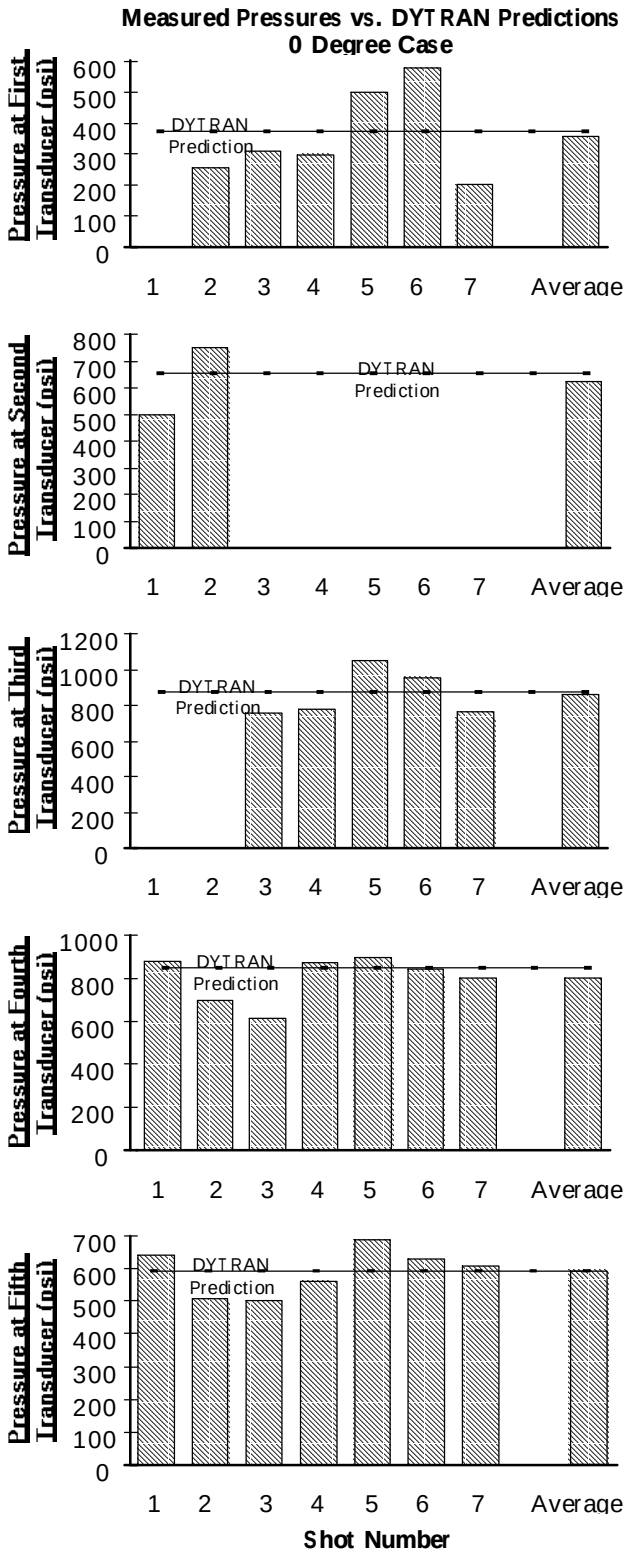

Fig. 8. Comparison of peak pressure at various transducer locations.

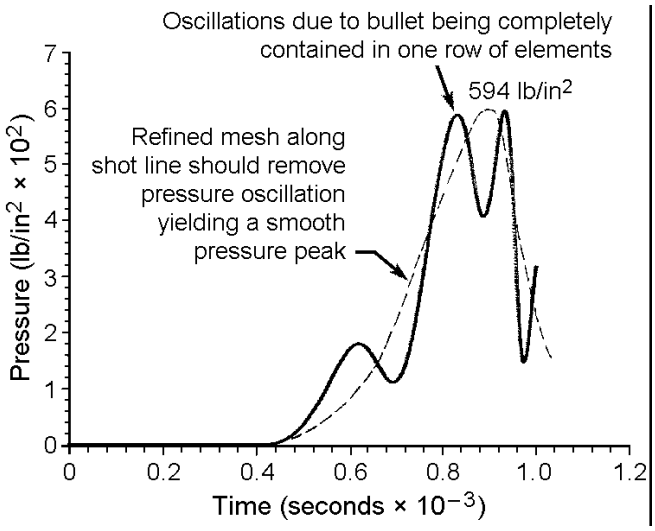

Fig. 9. MSC/DYTRAN™ pressure time history for the fifth pressure transducer.

ballistic test results, simulations will be used for pre-test guidance in positioning the shotline axis.

Composite Wing Test Specimens

The composite wing test specimens were built and tested under the DMLCC–BW contract by Bell Helicopter Textron, Inc. for Wright Laboratory (Ref. 2). Each composite wing panel is 41 inches long and 48 inches wide (1.04 m × 1.22 m), with curved aerodynamic surface representing upper wing skin. These skin panels are cocured with five stringers and composite ribs bonded to the panels. The panels are individually mounted onto the open side of the aluminum test box to simulate a wing fuel bay of an aircraft as shown in Fig. 14 (from Ref. 9). The composite panels with bonded ribs are mechanically fastened to the rib webs and front/rear spar webs of the test box.

A crash-resistant self-sealing fuel cell was installed in the test box before each ballistic test and the fuel cell is filled with water, leaving approximately a 10% ullage. Ballistic foam was used to fill the volume between the stringers, support the fuel cell, reduce the probability of dry bay fire, and mitigate hydraulic ram damage to the surrounding structure.

Four high-speed pressure transducers were installed on the inside wall of the fuel cell closest to the composite test panels. Two rosette strain gages were mounted to each stringer lower cap; rosette strain gages were also mounted to the outer skin surface directly above the stringer strain gages.

All three shots impacted the aluminum box first and traveled through the water-filled fuel cell before exiting through

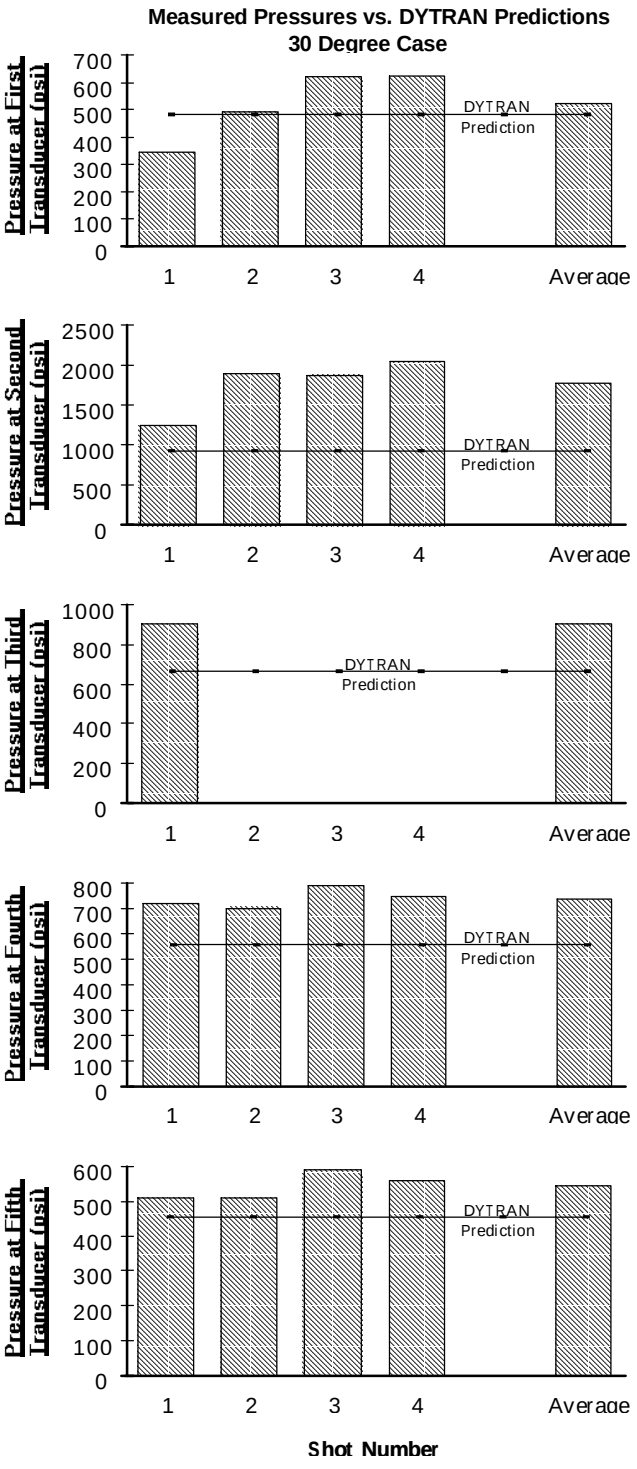

Fig. 10. Comparison of peak pressure at various transducer locations.

the composite test panels. The first two shots used a small bore projectile fired at 25-deg and 45-deg obliquity to the aluminum panel. Their trajectories through the water induced complete tumbling causing the projectile trajectories

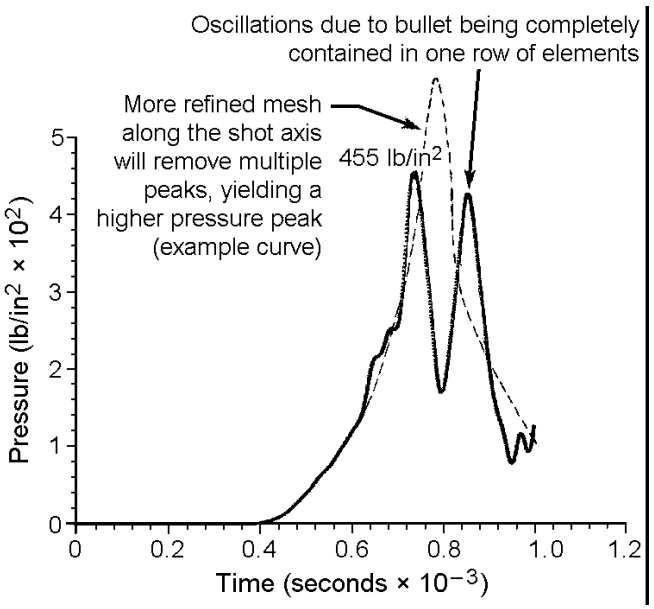

Fig. 11. MSC/DYTRAN™ pressure time history for the fifth pressure transducer.

to deviate from the shotline and exit through the composite skins rather than a stringer. Thus no structural damage occurred to the stringer, and only a limited damage occurred to the skin. To improve the likelihood of impacting a stringer on the exit panel and cause maximum possible damage, a large bore AP projectile was used for the third shot. This third ballistic test shot was simulated with MSC/DYTRAN™.

A model of the composite wing used for this simulation is shown in Fig. 15. In this model, the wing structure is connected to adjacent ballistic foam through physical connection at common grids. The ballistic foam and fuel cell wall are connected with a rigid connection. The fuel cell wall interacts with fuel through ALE coupling. The interaction between the fuel and projectile is defined using a general coupling. Two adaptive contacts are used to model the interaction between the projectile and entry and exit sides of the wing structure. An adaptive master/slave contact models the interaction of projectile with the fuel cell wall. In addition, the model contains the following entities.

Fluid Model. The water in the fuel cell is modeled using 51,199 Eulerian hydrodynamic elements with a density equal to water. The air in the 10% ullage is modeled using void material properties for the corresponding hydrodynamic elements. The Euler mesh is composed of two distinct regions: a central finely-meshed region around the shotline and a surrounding region (with mesh gradually becoming coarser) extending to the fuel cell walls.

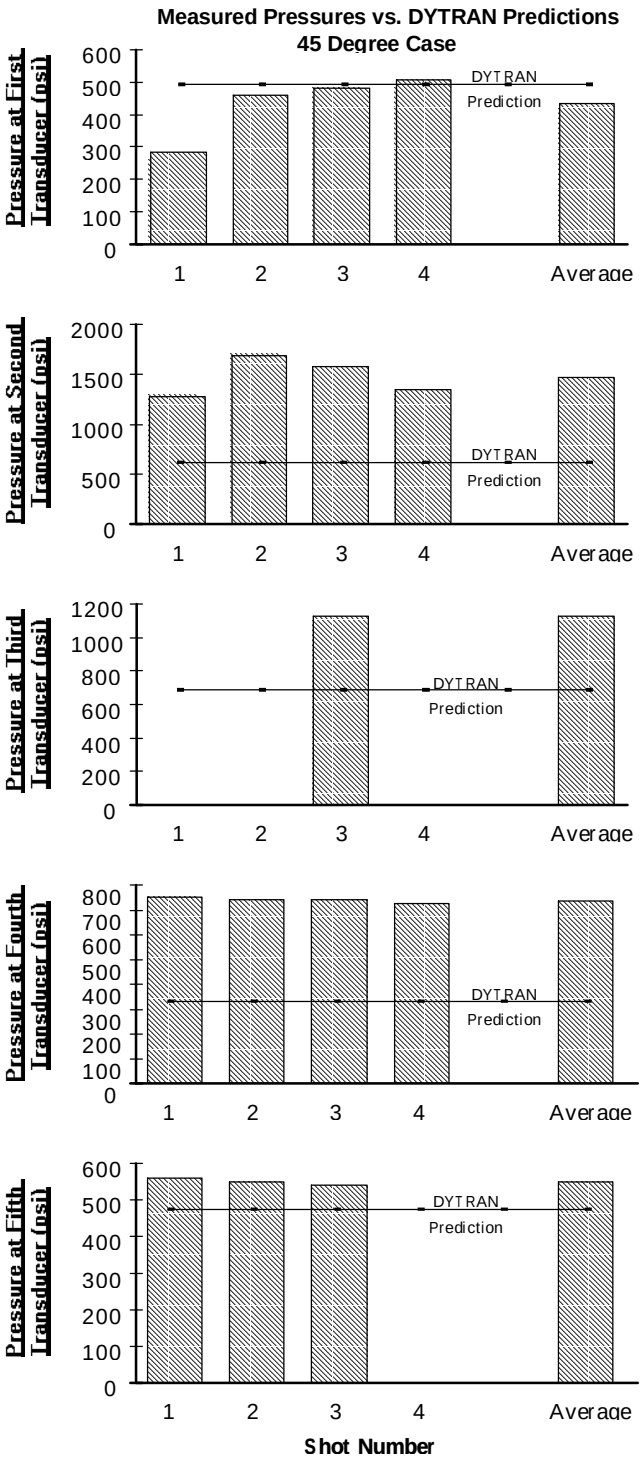

Fig. 12. Comparison of peak pressure at various transducer locations.

Composite Wing Model. The composite panel representing upper wing skin in Fig. 14 is modeled with 5,478 composite Lagrangian shell elements with orthotropic material properties. The stringers are modeled with rod elements. The aluminum test box is modeled using 5,428

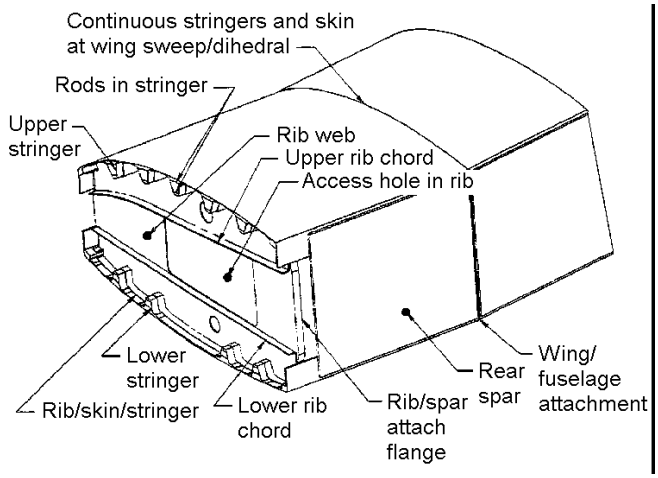

Fig. 13. Composite bonded wing – isometric view (from Ref. 7).

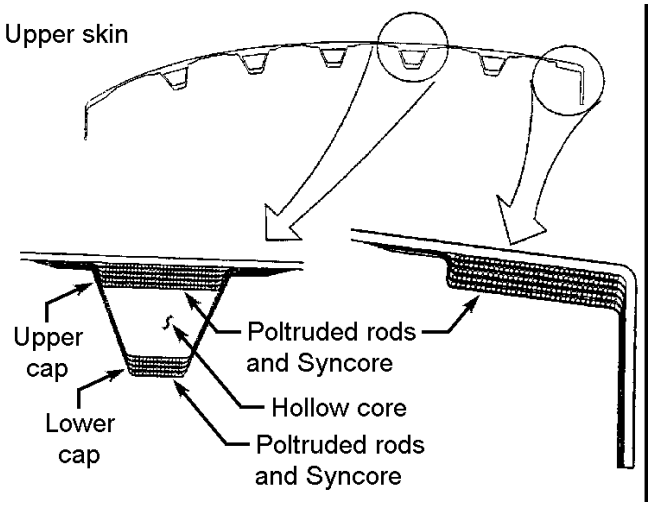

Fig. 14. Pultruded rod packs for stringers and corner flanges (from Ref. 7).

Lagrangian shell elements having properties representing the 0.160-inch-thick (4.06-mm) aluminum plate.

Ballistic Foam Model. The ballistic foam is modeled using 4,704 Lagrangian solid elements with the properties of crushable foam, which fills the space around the fuel cell between the stringers and the aluminum test box. The primary purpose of this ballistic foam is to support the fuel cell.

Fuel Cell Model. The fuel cell wall is modeled using 7,680 Lagrangian shell elements with elastoplastic material properties. The actual material of the wall was tested to determine its stress-strain properties, which were then used in elastoplastic material property information tables.

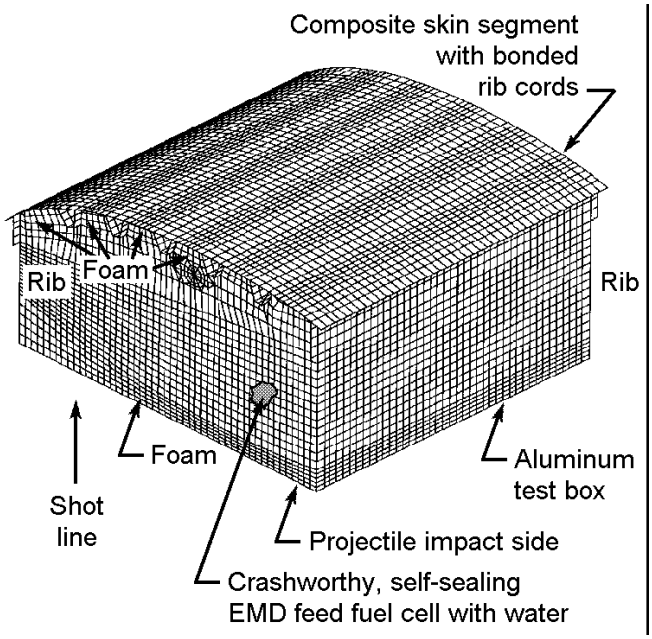

Fig. 15. Composite wing test article MSC/DYTRAN™ model.

Projectile Model. The large bore projectile is modeled with 240 Lagrangian shell elements. These elements define the shape of the bullet surface, which for the current simulations is defined as rigid. The mass of the projectile was obtained from Ref. 6; however, the moments of inertia had to be computed, since the MATRIG feature was not used. No yaw perturbation is specified for the initial condition at wing box penetration.

Analytical Results. The MSC/DYTRAN™ simulation of the large bore projectile impact at 2,605 ft/s (794.0 m/s) and 0-deg obliquity indicates that the projectile trajectory and the location of the projectile exit (Fig. 16) closely match those observed in the test. The projectile stays nearly aligned after it travels through the fuel cell (i.e., there was almost no tumbling) and impacts the cap on the bottom stringer at the outboard lower area of the skin panel nearly 9 inches (0.23 m) from the rib bond. The projectile exits in the analysis with a velocity of 2,068 ft/s (630.3 m/s), compared with the 1,976 ft/s (602.3 m/s) measured in the test (a 4.7% difference). The reduced exit velocity in the simulations is partly due to the removal of fuel cell Lagrangian elements from the bullet path to ensure that the ALE surface would not degenerate.

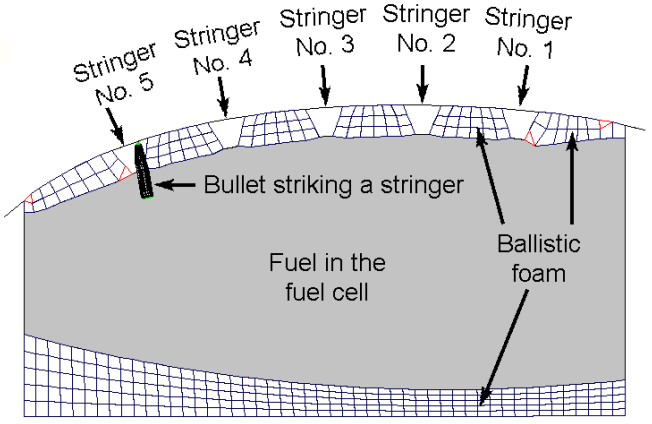

Fig. 16. MSC/DYTRAN™ model showing projectile exit location for Shot No. 3.

Pressure data at two of the four transducers was unreliable. Pressures in the Euler elements closest to the two functioning transducers are 172 psi (1,186 kPa) and 750 psi (5,171 kPa). In the ballistic test data, these pressure readings measured 306 psi (2,110 kPa) to 546 psi (3,765 kPa). Only approximate locations for the pressure transducers were available and, due to the finer hydrodynamic mesh in the region of the transducers, there may be a possible discrepancy in the location of the transducers in the Euler mesh. This may explain the difference between measured and computed pressures.

Damage from the ballistic test was limited to one end of the skin panel near the projectile exit location. Simulation indicates the largest microstrain (με) is 2.625 με tension and 5.017 με compression, compared with 1.764 με tension and 4.241 με compression measured from the corresponding strain gages in the test. Distortional energy contours from the simulation results, shown in Fig. 17, indicate limited failure of the stringers is likely.

In the test results, the hydraulic ram pressure delaminated a portion of the forward spar cap. The analysis results of Fig. 18 confirm that the rib flange had high strain levels representative of failure near the forward spar cap.

The high strain contours shown in Fig. 18 correspond closely with the visible bond failure observed in the ballistic test. Strain levels in the analysis are high near the center stringers and along the skin surface between the two lower stringers. Lower strain levels exist in the analysis around the remaining stringers, indicating a good probability of being able to carry load. This agrees with high-speed film from the test, which indicates that a bond line separation was induced during the test, but did not propagate substantially.

As in the case of the generic tank, the physics of ballistic dynamics phenomenon are closely replicated for the composite wing tank. Thus MSC/DYTRAN™ has the potential of being a useful design tool for enhancing ballistic tolerance.

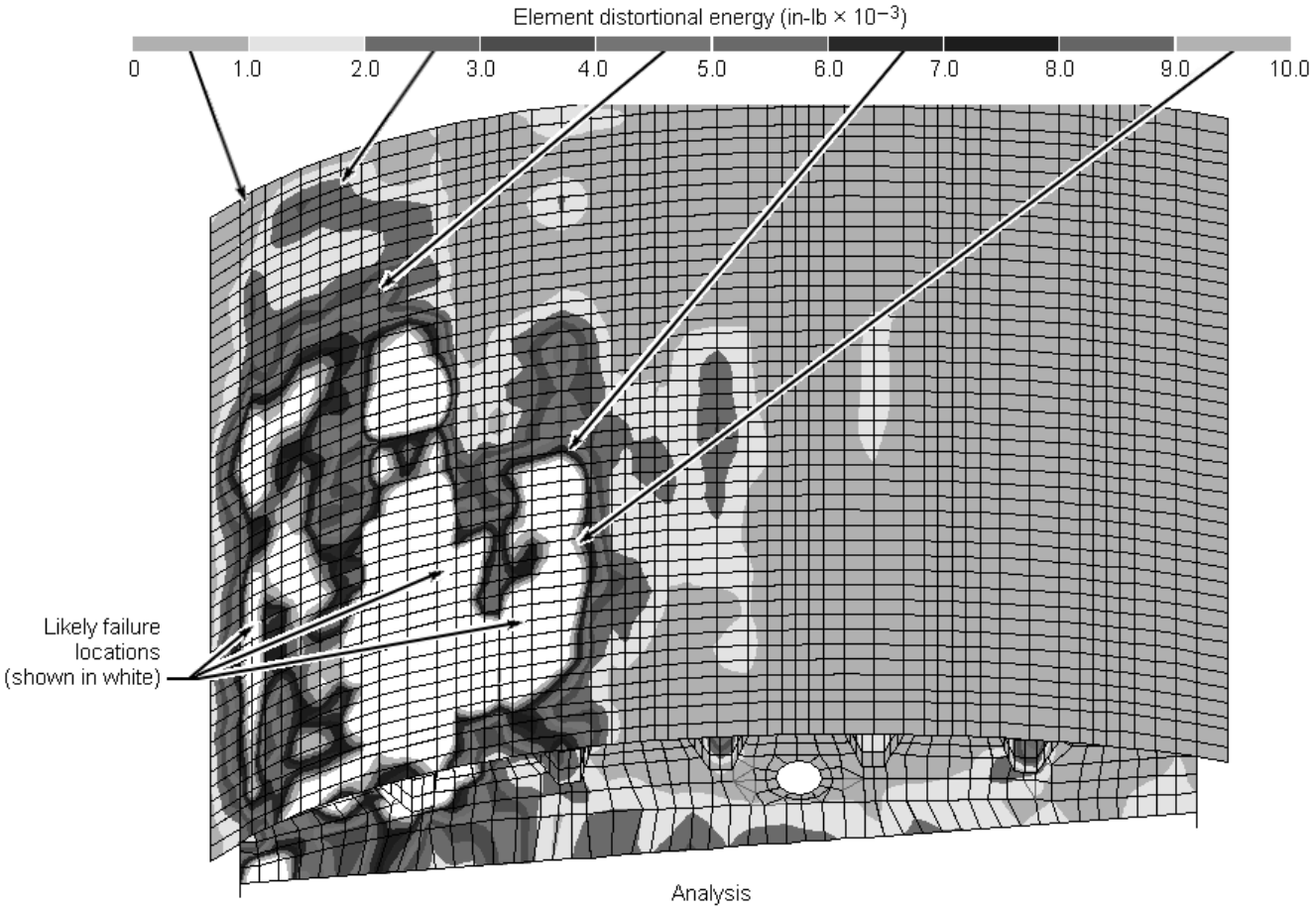

Fig. 17. Failure locations from Shot 3 ballistic simulation.

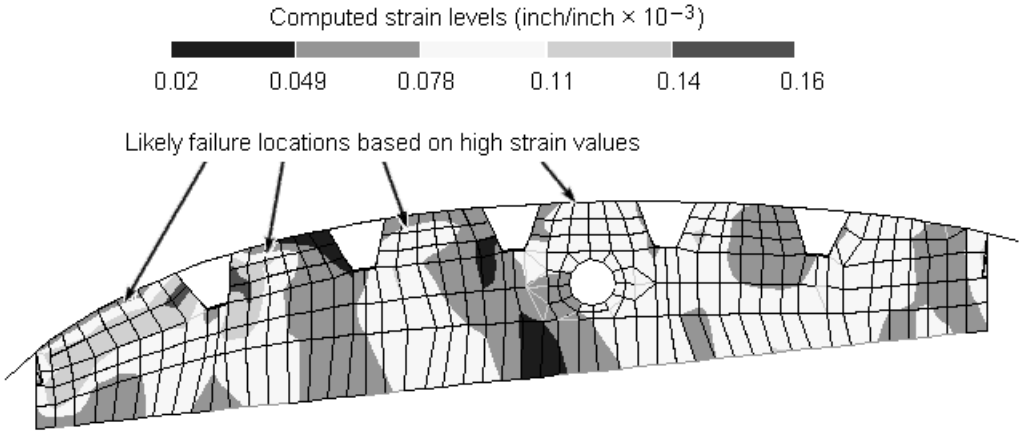

Fig. 18. Strain contours on the wing rib for Shot 3.

CONCLUSIONS AND RECOMMENDATIONS

Based on the ballistic simulations conducted herein, MSC/DYTRAN™ appears to be a promising tool for improving ballistic tolerant designs and in guiding pretest specimen setup. Specifically, the following conclusions are drawn:

a. The ballistic analyses conducted demonstrate that MSC/DYTRAN™ can be used to directly simulate the full sequence of hydraulic ram, including the initial shock phase.

b. The ballistic simulations evaluated indicate that MSC/DYTRAN™ can be effectively used to predict projectile trajectories and tumbling behavior. This is essential for an analytical tool during pretest setup to ensure projectile strike and exit at critical locations.

c. Calculated peak overpressures agree closely with measured data (within 5% for the generic case studied) for projectiles that do not tumble early in the sequence. However, pressure correlation is strongly affected by mesh density, especially for projectiles that do tumble early, such as those with high obliquity.

d. In the area of structural integrity and failure prediction, more evaluation is necessary, since a refined mesh is expected to improve accuracy in the fluid pressures, which serve as a dominant mechanism for structural loading. However, it does appear that better failure models for orthotropic materials are needed to assess failure mode prediction, specifically strain contours or delaminations. While MSC/DYTRAN™ contains many failure models for different modeling elements and for different material types, the failure mode prediction requires very detailed material data for most failure models, which may not always be available. Even though microstrain, stress, and distortional energy contours have been presented for the simulations, more work is required to have confidence in these predictions.

ACKNOWLEDGMENTS

The authors wish to thank the following individuals for their support of this effort: Robert V. Dompka, Jack R. Johnson, Ron Haker, and Andy T. Hill of Bell Helicopter Textron, Inc., Stewart W. Lilley, formerly of Bell Helicopter Textron, Inc,. and Arjaan Buijk of MacNeal-Schwendler Corp. Thanks are also due to Wright Patterson AFB, and particularly to Mr. Dick Holzwarth, technical coordinator for the DMLCC–BW ballistic test effort, which served as the basis for correlating the corresponding analysis.

REFERENCES

1. MSC/DYTRAN™ (version 2.3); MSC/DYTRAN™ is a registered trademark of the MacNeal-Schwendler Corporation, Los Angeles, California.

2. "Design and Manufacture of Low Cost Composites – Bonded Wing (DMLCC–BW)," Contract F33615-91C-5729.

3. Bharatram, G., Schimmels, S.A., Venkayya, V.B., "Application of MSC/DYTRAN to the Hydrodynamic Ram Problem," MSC User's Conference, Universal City, California, 1995.

4. Lee, T.W., "Preliminary Hydrodynamic Ram Investigations at Denver Research Institute," Hydrodynamic Ram Seminar, Technical Report AFFDL-TR-77-32, May 1977.

5. Lundstrom, E.A., and Fung, W.K., "Fluid Dynamic Analysis of Hydraulic Ram, IV, (User's Manual for Pressure Wave Generation Model)," prepared for Joint Technical Coordinating Group for Aircraft Survivability, Naval Weapons Center, China Lake, California, Report JTCG/AS-74-T-018, Sept. 1976.

6. Lundstrom, E.A., and Fung, W.K., "Fluid Dynamic Analysis of Hydraulic Ram, III, (Result of Analysis)," prepared for Joint Technical Coordinating Group for Aircraft Survivability, Naval Weapons Center, China Lake, California, Report JTCG/AS-74-T-015, Sept. 1976.

7. Lundstrom, E.A., Fluid Dynamic Analysis of Hydraulic Ram, NWC TP 5227, Naval Weapons Center (Unclassified), China Lake, CA, July 1971.

8. Nunn, K., Dompka, R., Jones, L., "Design and Manufacture of Low Cost Composites - Bonded Wing, Phase II, Final Report," WPAFB WL-TR-93-8009, Manufacturing Technology and Flight Dynamics Directorates, Wright Laboratory, Wright Patterson Air Force Base, Ohio, Dec. 1993.

9. Hill, A.T., "Hydraulic Ram Ballistic Testing of Low Cost Composite Wing Structure," presented at the 37th AIAA / ASME / ASCE / AHS / ASC Structures, Structural Dynamics, and Materials Conference, Salt Lake City, Utah, April 15–17, 1996.